Deciphering the Electrocatalytic Reactivity of Glucose Anomers at Bare Gold Electrocatalysts for Biomass-Fueled Electrosynthesis

Yaovi Holade, Hazar Guesmi, Jean-Sébastien Filhol, Qing Wang, Tammy Phang, Jad Rabah, Emmanuel Maisonhaute, Valérie Bonniol, Karine Servat, Sophie Tingry, et al.

Deciphering the Electrocatalytic Reactivity of Glucose Anomers at Bare Gold Electrocatalysts for Biomass-Fuelled Electrosynthesis

Yaovi Holade,[1,*] Hazar Guesmi,[2,*] Jean-Sebastien Filhol,[2] Qing Wang,[2] Tammy Pham,[3] Jad Rabah,[4] Emmanuel Maisonhaute,[4] Valerie Bonniol,[1] Karine Servat,[5] Sophie Tingry,[1] David Cornu,[1] K. Boniface Kokoh,[5] Teko W. Napporn[5,*] and Shelley D. Minteer[3,*]

[1]Institut Européen des Membranes, IEM, UMR 5635, Univ Montpellier, ENSCM, CNRS, 34090 Montpellier, France

[2]Institut Charles Gerhardt Montpellier, ICGM, UMR 5253, Univ Montpellier, ENSCM, CNRS, 34090 Montpellier, France

[3]Departments of Chemistry, University of Utah, Salt Lake City, Utah 84112, USA

[4]Sorbonne Université, CNRS, Laboratoire Interfaces et Systèmes Electrochimiques, 4 place Jussieu, 75005 Paris, France

[5]Université de Poitiers, IC2MP UMR-CNRS 7285, 86073 Poitiers Cedex 9, France

ABSTRACT. One of the questions not yet elucidated in the electrocatalytic oxidation of glucose is whether the first step of dehydrogenating proton-coupled electron transfer (PCET) concerns the hydrogen directly bound to anomeric carbon (β-anomer) or that bound to oxygen of the anomeric carbon (α-anomer). The knowledge is necessary for renewable-energy-powered electrosynthesis of chemicals/fuels. To decipher that, we have used α-D-, β-D- and D-glucose

models to interrogate the electrocatalysis of the glucose anomers in neutral and alkaline pHs. We have also optimized a pulse methodology to directly grow surfactant- and binder-free gold particles onto the gas diffusion electrode (GDE) as freestanding electrocatalysts to bridge the scales between fundamental and applied research in fuel cells and electrolysis. Cyclic voltammetry measurements show that the electrooxidation of all the glucose anomers starts at a potential region where the gold surface is not yet fully oxidized and is dominated by the dehydrogenating adsorption of glucose, which rules out the hypothesis that glucose first adsorbs on hydroxylated gold surface. The results in neutral pHs highlight the better electrocatalytic reactivity of α-anomer over β-anomer and the opposite in alkaline pHs, which invalidates the traditional thoughts that the β-anomer would always be the most reactive. Potential-dependent energy profiles computed by density functional theory (DFT) mainly confirm the promoted approach by the OH of the anomeric carbon (α-anomer). The deciphering of the electrocatalytic reactivity of glucose anomers at GDE-Au electrocatalysts, where gluconate is the main oxidation product at high selectivity and faradaic efficiency (>80%), opens opportunities to stimulate the electrosynthesis of renewable platform chemicals from the cellulosic biomass. The high selectivity and faradaic efficiency towards gluconate, a commodity renewable chemical, opens opportunities to stimulate the biomass-fuelled electrosynthesis.

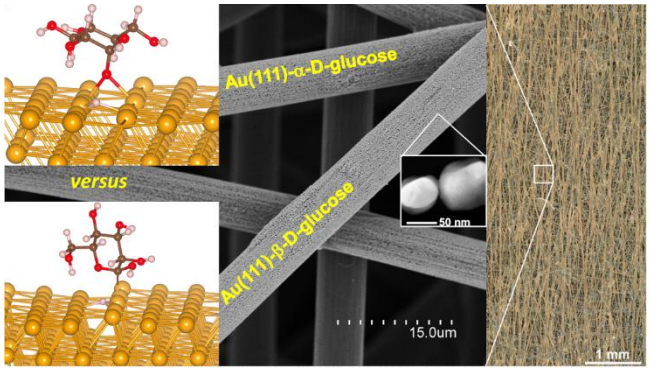

Table of Contents (TOC) graphic.

KEYWORDS: gold nanoparticles, gluconic acid, carbohydrates, biomass conversion, gas diffusion electrode, electrodeposition, electrocatalysis, density functional theory.

1. INTRODUCTION

Over the last decades, the (bio)electrocatalysis of glucose has been aiming to harvest electrical energy from (bio)fuel cells for powering small devices.[1-2] Recently, the (bio)electrooxidation of glucose has appeared as a powerful tool for the electrosynthesis of important commodity chemicals (gluconate, etc.) to manufacture biodegradable polymers, detergents, soaps, food ingredients, etc. in a green fashion with low environmental impacts.[3-5] Indeed, glucose is the monomer of cellulose, the most abundant biopolymer accounting for 35-50% of the total biomass. Hence, the fundamental understanding of its (electro)catalytic reactivity is of even more importance as it bridges the gap in understanding the reactivity and valorization of the cellulosic biomass.[4,6] Today, in order to achieve real devices, a better knowledge of how glucose reacts is missing for a better control of the selectivity at high current density and of the stability of the whole process.

The most debated fundamental question regarding the glucose oxidation on catalytic surfaces is whether the initial proton-coupled electron transfer (PCET), is the dehydrogenation of anomeric carbon (C–H activation, α-anomer) or the deprotonation of hydroxyl group bound to anomeric carbon (O–H activation, β-anomer). Indeed, the spontaneous closing of the glucose ring via hemiacetal bond results in an additional source of isomer on the anomeric carbon referred to as α-D- and β-D-glucopyranose (Scheme 1), the main constituents of glucose; in blood plasma, α-D:β-D ratio is 1:2.[7-8] We note that, among the three natural forms of glucose, β-D is 30 and 102 times as costly as D and α-D, respectively. Seminal enzymatic studies support that glucose oxidase (GOx) catalyzes only β-D anomer (the monomer unit in cellulose) oxidation into gluconate, which means that before use, α-D anomer (the monomer unit in starch) and D-glucose (mixture of α-D and β-D) forms need to be isomerized first.[7,9-11] Thus, the high price of

β-D anomer has made D-glucose the most used in research fields; and in bioelectrochemistry precisely, it has become an accepted rule to wait several hours to achieve equilibrium because of the widespread opinion on that better reactivity of the β-D anomer.[7,9-11] These traditional thoughts were extended to abiotic electrocatalysis with bulk electrodes,[12] additionally arguing that due to the axial and equatorial positions of H/OH groups on anomeric carbon, β-D configuration would be the most favorable to approach a catalytic surface (Scheme 1), which could be true for biocatalysis where the active site is often buried in a bulky tridimensional network.[11] However, huge gap of knowledge exists about nanostructured electrodes used in real devices of energy conversion and electrosynthesis.

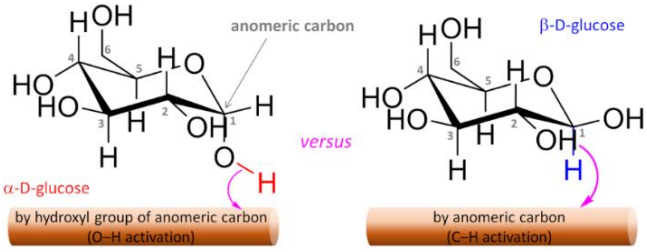

Scheme 1. Illustration of the two possible initial steps during the PCET by considering the chair conformations of α-D (left) and β-D (right) glucopyranose electrooxidation by its anomeric carbon. We note that glucose molecules mainly exist (99%) as pyranose forms in aqueous solution.

Hsiao *et al.*[13] investigated the electrooxidation of glucose in phosphate buffered solution (PBS, pH7.4) on bulk gold, and found that the rate-determining step (*rds*) is the C−H bond cleavage, that is, a better reactivity of the β-anomer. However, they omitted to compare the electrochemical responses of the three forms of α-D-, β-D- and D-glucose. Largeaud *et al.*[12] found that at 2 °C, β-D-anomer has the highest electrocatalytic reactivity at bulk Pt. However, the conclusion is limited to 2 °C and no experiment was performed in neutral pHs or with Au

which is expected to be the best catalyst for the selective electroconversion of (oligo)saccharides by their anomeric carbons.[14] According to density functional theory (DFT) calculations with Au and Pt atoms-doped graphene surfaces,[15] glucose molecule approaches the surface through the α-anomer, which contradicts the above results while the step of O–H bond breaking was not investigated, which prevents any extrapolation of what happens after the PCET. Ishimoto *et al.*[16] proposed that glucose first adsorbs on hydroxylated gold surface, which is in contrast with experimental observations showing that glucose oxidation starts when the surface is not yet fully oxidized (< 0.3 V_{RHE}).[17-20] DFT studies at 0 V_{SHE} proposed that the glucose electrooxidation starts by the deprotonation of OH group bonded to anomeric carbon,[21] however, did not address the central question of the effect of an electrode potential on the intermediates' energy profiles. These theoretical results contradict seminal experimental data and other DFT works from groups of Greeley[22] and Koper[23] showing that among C–H, O–H, and C–C bonds, the C–H bond scission is the easiest. So, it becomes necessary to perform an extensive experimental and theoretical investigation of all the three forms of α-D, β-D and D-glucose to clearly decipher the electrocatalytic reactivity of glucose anomers.

A fair assessment of the intrinsic electrocatalytic properties of a glucose molecule with a gold surface requires the use of bare (organic ligand-free) particles because any surface contaminant severely alters the trends.[24] Besides, the use of three-dimensional electrically conductive gas-diffusion electrode (GDE) should enable to better manage the mass transport and target higher current densities.[25] However, for gold, we still lack methodology to control the growth towards particles with clean surfaces at low metal loading onto GDE. To fill the above gaps in fundamental knowledge on the electrocatalysis of glucose's anomers, we report the novel synthesis of bare and free-standing GDE-Au electrocatalysts, electrochemical and computational

interrogations. In the present context of rush towards glucose analogues to lower the electrolyzers' energy cosumption,[3-5,26-27] our experimental and theoretical studies provide the basis to understand the catalytic reactivity and to guide the design of efficient electrodes.

2. RESULTS AND DISCUSSION

Free-standing Electrocatalysts: Morphology and Structure. We designed a methodology to directly grow Au particles onto a GDE (Figure 1a) without any use of an organic capping agent/surfactant or the addition of an ionomer prior to electrochemical tests. Our choice of gold as electrode material was guided by preliminary thermodynamic and kinetic tests (Figures S1-S2). The optimized methodology is the pulsed galvanostatic reduction of $AuBr_4^-$ (Figures 1a and S3) composed of an OFF step [open circuit potential (OCP) i.e. I_{OFF} = 0, t_{OFF} = 5 s, relaxation], an ON step (I_{ON} = -2800 µA, t_{ON} = 5 s, deposition] and repeated 180 times to synthesize GDE-Au_-2800µA. With total electrical charge unchanged, GDE-Au_-70µA, GDE-Au_-280µA, and GDE-Au_-4500µA were used to study the impact of the current. The profile of E(t) suggests that the relaxation is central to replenish $AuBr_4^-$ reagent in the vicinity of the electrode. Bromide regulates the nucleation and growth of Au seeds into particles,[28-29] and is easily removed by washing with water. The reddish color in Figure 1b evidences the presence of gold. To track the change in particles' morphology and size, we used scanning electron microscopy (SEM, Figures 1c and S4-S13). The results prove that the magnitude of the current is a powerful tool to regulate the nucleation and growth of Au seeds into particles of optimized sizes without any organic surfactant, which is very important for better electrocatalysis.

The crystallinity was confirmed by X-ray diffraction (XRD, Figure S14a) where the full width at half maximum is larger for GDE-Au_-2800µA/-4500µA than GDE-Au_-70µA/-280µA, which

confirms the decrease in the crystallite size as revealed by SEM. For in-depth studies, we next selected GDE-Au_-2800µA that has the best compromise between the particles' distribution over the electrode surface and the synthesis conditions. From energy-dispersive X-ray (EDX) data (Figure 1d, S12-S13 and Table S1) and X-ray photoelectron spectroscopy (XPS, Figures S14b-d), only metallic gold is formed because C and O come from the GDE and O may result from the natural oxidation when a metal is exposed to ambient air. The metal loading by inductively coupled plasma optical emission spectrometry (ICP-OES, Table S2) is as low as 0.54 wt.% (49 μg_{Au} cm^{-2}). Atomic force microscopy (Figures S15-S16) confirms the formation of 30-150 nm sized particles and highlights the increase of the average surface roughness R_a from 14.8 nm (GDE) to 33.4 nm (GDE-Au), that is, 126%, so an augmented active surface area (confirmed by electrochemistry).

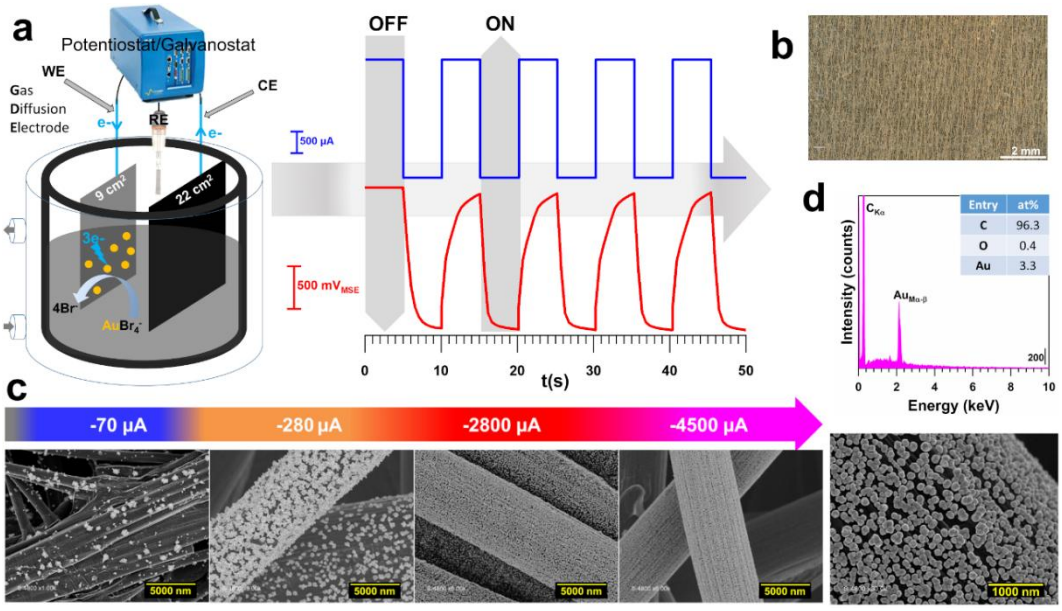

Figure 1. Synthesis of free-standing GDE-Au materials. a) Developed methodology to electrochemically grow Au particles onto GDE by galvanostatic pulses (parameters: $t_{ON} = t_{OFF} =$ 5 s, $I_{ON} = -2800$ µA, $I_{OFF} = 0$ µA, $\Sigma(t_{ON} + t_{OFF}) = 1800$ s). b) Optical microscopy of GDE-Au

(I_{ON} = -2800 µA). c) SEM images of GDE-Au for four values of I_{ON}. d) EDX pattern of GDE-Au (I_{ON} = -2800 µA).

Figures 2a and S17 show the prepared sample using a focused ion-beam dual-beam (dbFIB) microscopy. Figure 2b confirms a quasi-spherical morphology of particles with a size below 200 nm. The nanobeam diffraction pattern in Figure 2c confirms the polycrystalline structure of gold. Figures 2d-c reveal the surface orientation to identify the exposed facets which will interact with glucose anomers.[19,21] The interplanar space of 0.24 nm corresponds to (111) surface while (110) has an interplanar space of 0.29 nm. The lead underpotential deposition (Pb_{UPD})[17,20,29] experiments by cyclic voltammetry (CV) of Figures 2e-f validate the above results for both GDE-Au and bulk Au. Figures S22-S23 demonstrate that the bromide anion triggers the predominance of (111).[28,30]

The above results confirm our ability to synthesize bare (organic ligand-free) and free-standing GDE-Au electrocatalysts, which is important not only fundamentally to access intrinsic electrocatalytic activity, but also to be implemented into real applications of electrolyzers. Indeed, electrocatalysts are currently pre-made as a powder or liquid sample before drop-casting onto conductive supports such as glassy carbon or metal foams. However, the use in electrolyzers or fuel cells requires GDE during the membrane-electrode-assembly (MEA) in order to better manage the mass transport and target higher current densities.[25,31] As a consequence, the assessed intrinsic properties from half-cell with catalytic inks coated onto flat substrates do not reflect the effective performance of electrolyzer.[31-32] We note that to maintain satisfactory performance, the MEA step often requires to use too high metal loadings (hundred to even thousands of micrograms per square centimeter of electrode) to mitigate the often loss of electrocatalysts. To date, among the methods of growing electrocatalysts directly on the supports

to reduce the metal loading and to augment the durability (atomic layer deposition,[33] electrospinning,[34] reactive spray deposition,[35] chemical/hydrothermal[36]), electrodeposition is suitable approach.[37] The present optimized pulse electrodeposition methodology to directly grow surfactant- and binder-free gold particles onto the GDE as freestanding electrocatalysts should allow bridging the scales between fundamental and applied research in fuel cells and electrolysis.[25,31,38]

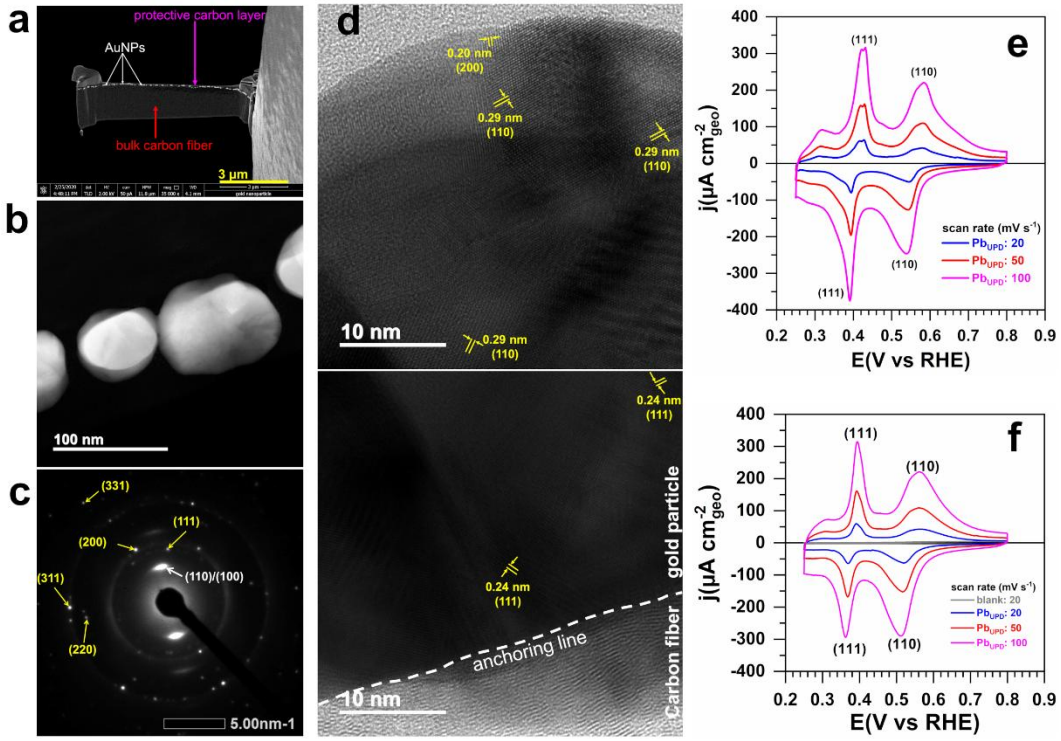

Figure 2. Structural characterization. a) Backscattered SEM image during the dbFIB preparation. b) HAADF-STEM image. c) NBD patterns. d) HRTEM images highlighting the "Au-carbon" interface and arrangements of Au atoms. (e, f) CVs of Pb_{UPD} at different scan rates (0.1 M NaOH, 1 mM $Pb(NO_3)_2$, 25 °C), GDE-Au *vs* Au bulk: e) As-synthesized GDE-Au and f) Au bulk.

Electrocatalytic and Electroanalytical Evaluation. We first used a neutral medium that kinetically reduces mutarotation to interrogate any reactivity difference between D-, α-D-, and β-

D-glucose (Tables S4). Polarimetry data (Table S5) show that a solution prepared from α-D-glucose contains 94.1 ± 0.3 % of α-D anomer while a solution prepared from β-D-glucose contains 97.4 ± 0.4 % of β-D anomer (that of D-glucose contains 98.9 ± 0.1 % of β-D anomer). These results and ref.[12] validate phosphate buffered solution (PBS, 0.2 M, pH7.4) as electrolyte to decipher the electrocatalytic reactivity difference between D, α-D, and β-D. Voltammograms of Figure 3a (as-synthesized GDE-Au) and Figure 3b (bulk Au) show that while the onset of electrooxidation is almost the same, 0.2 V_{RHE}, the peak current density trend is α-D > β-D > D. It is confirmed by the electrochemical impedance spectroscopy (EIS) where Figure 3c (details in Figures S24-25) at 0.5 V_{RHE} indicate that the origin of the high electrocatalytic reactivity of the α-D results from the reduced charge transfer resistance (R_{ct}); R_{ct} is 6542, 12704 and 16051 Ω cm^2, for α-D-, β-D- and D-glucose, respectively (Table S6). The behavior of the D-glucose in neutral electrolyte at both GDE-Au and Au bulk electrodes at different concentrations is presently unexplained as by considering the predominance criterion, the trend on the maximum current of D-glucose should be intermediate to that of α-D and β-D. It might be interesting to compare the behavior of D-glucose with physical mixtures of α-D and β-D (ideally at the same optical activity), which is beyond the scope of the present work. The logic is however verified in alkaline electrolyte as we see it for the Figures 3d and 3e. The plausible explanation would be the complexity of the electrolyte (NaOH *vs* PBS) and the kinetics of the mutarotation equilibrium compared to the basic medium since the difference is attenuated when testing the aged solutions.

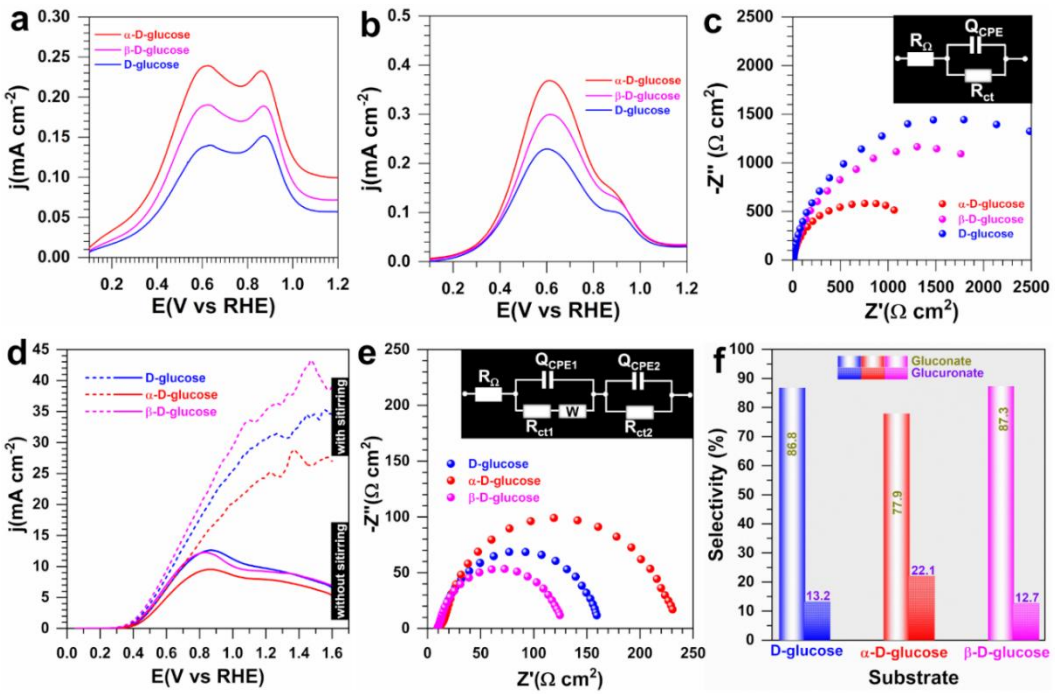

Figure 3. Electrocatalytic performance in alkaline and neutral media. (a, b) Background current corrected voltammograms [100 mV s^{-1}, 0.2 M PBS (pH7.4), $C_{glucose}$ = 10 mM, 25 °C] for D-, α-D-, and β-D-glucose: (a) As-synthesized GDE-Au and (b) Au bulk. (c) Complex-plane Nyquist impedance for Au bulk: inset is the equivalent electrical circuit at 0.5 V_{RHE} [0.2 M PBS (pH7.4), $C_{glucose}$ = 10 mM, 25 °C]. (d) Comparative voltammograms for D-, α-D-, and β-D-glucose [100 mV s^{-1}, 0.1 M NaOH (pH 12.8), $C_{glucose}$ = 0.1 M, 25 °C] without stirring, and with stirring for as-synthesized GDE-Au. (e) Complex-plane Nyquist impedance: inset is the equivalent electrical circuit at 0.34 V_{RHE} for D-, α-D-, and β-D-glucose [0.1 M NaOH (pH 12.8), $C_{glucose}$ = 0.1 M, 25 °C]. (f) Product distribution from HPLIC after bulk electrolysis of D-, α-D-, and β-D-glucose [0.1 M NaOH (pH 12.8), $C_{glucose}$ = 0.1 M, gentle solution stirring].

Based on the Tafel slope of 159-186 mV dec^{-1} (Figures S24c and S25c), Scheme S1 and Figure S24e, the limiting step is the first PCET of glucose dehydrogenation (Volmer reaction[39]). Control experiments after 18 hours of equilibrium (Figure S25) highlight a decrease of the peak

current density of α-D while that of β-D and D increases, thus underpinning the conclusion that in neutral pHs, α-D-glucose is the most reactive anomer. We note that, the electrooxidation starts in a potential region where gold is not yet fully oxidized (Figures S24-S25), however, the reactivity of glucose at gold was assigned to oxidized-like surface.[13] The absence of hydroxyls on gold surface promotes a glucose approach by the OH group bonded to hemiacetal carbon. This situation might be different in alkaline pHs where the surface oxidation results from the adsorption of OH^- of the electrolyte while acidic or neutral pHs require to split H_2O (solvent). Indeed, glucose mainly exists as pyranose form in aqueous solution (more than 99%; less than 0.5% for the linear form and furanose forms exist in negligible amounts) so that the most favorable structures is the chair conformations of α-D and β-D-glucopyranose (simply referred to as α- or β- D-glucose) that differ by the configuration of a stereo-center (anomeric carbon, carbon at C1 position, Scheme 1). Corollary, there are at least two reasons for the electrocatalytic reactivity discrepancy between the α-D and β-D forms. First, α-D in a chair conformation should approach a catalytic surface by its –OH group linked to the anomeric carbon, which results in a O–H dehydrogenation/PCET. This means that β-D in a chair conformation should approach a catalytic surface by its –H group linked to anomeric carbon (C–H dehydrogenation/PCET). The second reason is related to a hypothetical structure rearrangement by rotating before the adsorption to offer a better exposure of the functional group to the electrocatalytic surface, which is very unlikely because it would require much energy so that it is less evoked in the literature.[12-13,15-16,21] Our present data in PBS (0.2 M, pH7.4) demonstrate that, for the experimental conditions where the population of surface hydroxylated species is low (due to pH and/or low electrode potential), the highest activity results from the activation of α-D-glucopyranose by its O–H bonded to the anomeric carbon (Scheme 1). This dehydrogenation/PCET results in an

oxidized-like surface. For alkaline media where the electrode surface is densely surrounded by hydroxylated species, an –H approach should prevail.

Before examining that hypothesis in alkaline electrolyte, we established a baseline by using D-glucose to compare the as-synthesized GDE-Au free-standing electrodes at four pulsed currents with commercial Vulcan-supported Au (Figure S26a-f) and literature (Table S7). GDE-Au_-2800µA is the most efficient by the metrics of current density per geometric area (mA cm^{-2}_{geo}), per weight (A g^{-1}_{Au}) and per ECSA of the active metal (mA cm^{-2}_{Au}). Specifically, GDE-Au_-2800µA has a peak current density (256.4 A g^{-1}_{Au}, 12.6 mA cm^{-2}_{geo}) that surpasses the commercial Vulcan-Au (177.7 A g^{-1}_{Au}, 8.7 mA cm^{-2}_{geo}). The specific current density is 10-times higher for GDE-Au_-2800µA (7.8 mA cm^{-2}_{Au}) than Vulcan-Au (0.8 mA cm^{-2}_{Au}) (Figure S26a). The achieved j_p = 7.8 mA cm^{-2}_{Au} outperforms the reported j_p = 1.6 mA cm^{-2}_{Au} for AuAg nanoporous sponges.[40] The comparison with relevant nanocatalysts (Table S7) where j_p is typically 0.4-20 mA cm^{-2}_{geo} (0.7-600 A g_{Au}^{-1} for 14-200 μg_{metal} cm^{-2}) shows that the present GDE-Au is superior with 49 μg_{metal} cm^{-2} only[18,26,40] because of the absence of organic surfactants at the surface of the particles and the strong Au-support interaction. Bulk electrolysis (Figures S28-S32, Table S8) and high-performance liquid ionic chromatography (HPLIC) showed gluconate as the main product with a selectivity of 84-97 % and a faradaic efficiency of 61-88% depending on the used method of electrolysis. These data and post-mortem analysis (Figures S36-S39, Table S9-S10) validate our initial hypothesis that the direct growth of gold on GDE allows targeting not only a better catalytic activity, but also a better stability. Hence, we can use the same method to electrocatalytically screen α-D and β-D anomers. We note that the rate of the glucose conversion into the corresponding products (gluconate or glucuronate) can readily be fixed by adjusting the area of the working electrode relative to the considered glucose amount

(concentration, volume), the duration of the electrolysis, the electrolyte concentration, etc. Table S8 shows that on can easily achieve nearly 65-69% from 42 mL of 0.1 M glucose with a working electrode area of 4.5 cm^2 by fixing current (j_{ON} = 10 mA cm^{-2}) or potential ($E_{ON} = E_{ox}$ = 0.8 V vs RHE) for 2 to 4 h (ON step during the pulsed method), which is promising.

The results in alkaline medium for D-, α-D- and β-D-glucose shown in Figures 3d-f (extended data in Figures S40-S47) highlight lower current densities for α-D-glucose regardless of the solution agitation to facilitate the mass transport. EIS at 0.34 V_{RHE} (Figure 3e, Table S11) indicates that the origin of the high current density results from the reduced charge transfer resistance. It results that, in alkaline pH, β-D-glucose is the most reactive anomer, i.e. an approach to the catalytic surface by the H bonded to the anomeric carbon. The Tafel slope (Figures S43-S45) is in the range of a Volmer reaction as the *rds* similar to neutral pH. Seminal studies suggest that the electrocatalytic activity of gold towards glucose oxidation results from the presence of $Au(OH)_x$ species.[13] Herein, the starting potential of E_{onset} < 0.3 V_{RHE} where the gold surface is free of hydroxyl/oxide suggests a possible contribution of the OH^- from the electrolyte based of the different scenarios of Scheme S1 (see Figure S40 for details). To avoid the nucleophilic attack of OH^- to the hemiacetal carbon leading to the conversion of glucose into carboxylate, aged solutions were not studied similar to neutral pH. We next performed the pulsed current electrolysis (PCE, I_{ON} = 10 mA cm^{-2}, Figures S46-47) in a H-type cell of the 3 forms of glucose to examine whether the selectivity is affected or not. Figure 3f displays the product selectivity (quantitative data in Table S12). The gluconate selectivity is 87% for D-glucose electrolysis (faradaic efficiency of 65%), 78% for α-D-glucose electrolysis (faradaic efficiency of 55%) and 87% for β-D-glucose electrolysis (faradaic efficiency of 66%). The high glucuronate selectivity of 22% for the electrolysis of α-D-glucose (i.e. an increase of 69%

compared to the 2 other substrates) means that the reactivity of the glucose by its terminal carbon is exacerbated for α-D-glucose which can also explain the difference in the electrocatalytic kinetics and the current density at high electrode potentials. The low conversions of glucose into the corresponding products (gluconate or glucuronate) from Table S12 are explained by the used short duration to probe the selectivity of D-, α-D-, and β-D-glucose since we have already achieved the proof of reaching high conversions with Table S8. So, similar to Table S8, high conversions could be obtained by adjusting the area of the working electrode relative to the initial glucose amount (concentration and volume) as well as the duration of the electrolysis, the electrolyte concentration, etc.

Control experiments on the capacity of the synthesized GDE-Au to transfer one electron by using the electrochemical redox probe $Fe(CN)_6^{3-}/Fe(CN)_6^{4-}$ show an ultrafast kinetics with a standard rate constant trend of GDE-Au [$k° = (7.9 \pm 0.6) \times 10^{-3}$ cm s^{-1}] > GDE [$k° = (0.8 \pm 0.1) \times 10^{-3}$ cm s^{-1}] and outperforms the commercial Vulcan-Au (Figures S48-S50 and Table S13-S14).

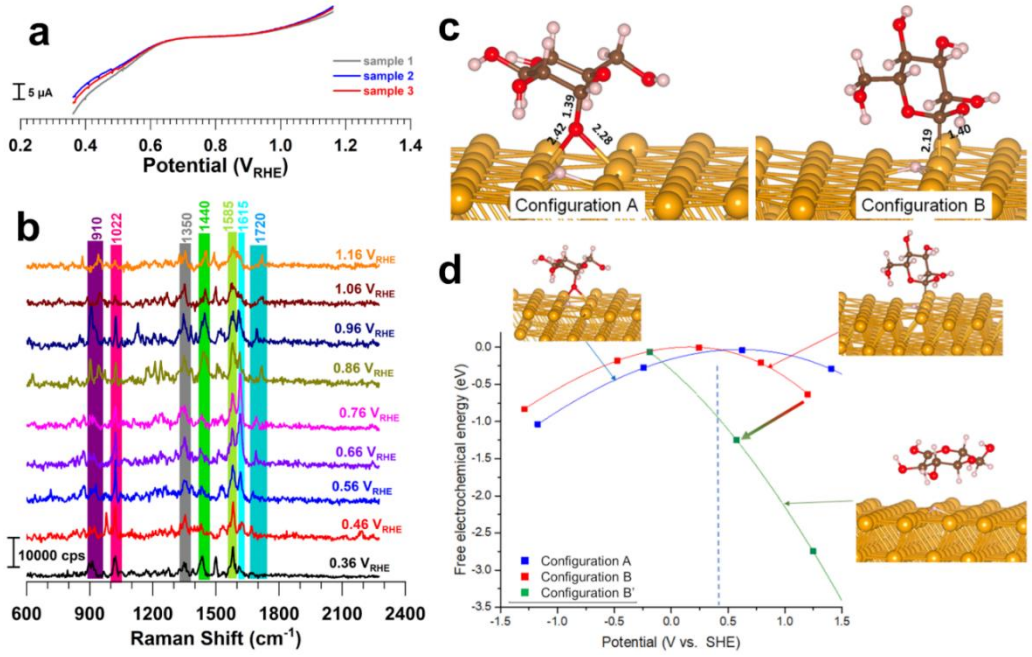

Figure 4. EC-SERS and DFT. (a, b) EC-SERS experiments in 0.1 M NaOH + 0.1 M D-glucose: (a) LSV at 10 mV s^{-1} for 3 different free-standing GDE-Au electrodes. (b) Raman spectra from EC-SERS. (c) Adsorption modes of O-dissociated form (configuration A) and C-dissociated one (configuration B) of glucose adsorbed on the Au(111) surface. The values indicate the Au-O, Au-C and C-O bond distances in Angstrom. (d) DFT calculated evolution of the free electrochemical energy of configurations A and B as a function of the applied potential. Planar configuration B' corresponds to the spontaneous rotation upon C-Au dissociation of configuration B. The color code is: Au atoms in yellow spheres, hydrogen in white, oxygen in red and carbon in brown.

In-situ Analysis: Electrochemical Surface-Enhanced Raman Spectroscopy (EC-SERS). We considered EC-SERS measurements on the free-standing GDE-Au electrocatalyst to decipher the interfacial structure of intermediates and products. SERS strategies were proposed to monitor glucose oxidation,[41-42] however, direct detection remains challenging and requires long acquisition times and/or high laser power. We overcome this challenge by focusing the laser on the GDE-Au electrocatalyst using a laser power of 0.375 mW and an acquisition time of only 1 s. The linear sweep voltammetry (LSV) of Figure 4a confirms the reproducibility. The graphitic structure of the GDE is characterized by D band (1350 cm^{-1}) and G band (1581 cm^{-1}) while glucose is characterized by its CH_2 wagging and bending of at 1330 cm^{-1} and 1436 cm^{-1}, respectively. Upon polarization (Figure 4b), there is an increase in intensity of some bands and the appearance of new bands due to the formation of oxidation products of glucose at the interface (details in Figure S51). The bands at 1585, and 1615 cm^{-1} belong to $\upsilon_{as}(COO^-)$ and those at 1440-1410 cm^{-1} for ν_s(O-C-O) suggest the formation of a carboxylate function.[42-44] Convoluted with CH_2 wagging and bending of CH_2,[41-42] we conclude that gluconate is the main

product because of the absence of CH_2 signal for glucuronate.[14,43] The band at 1720 cm^{-1} belongs to υ(C=O) of gluconolactone as reactive intermediate prior ring-opening and production of gluconate.[44-45] This study thus also reveals the exquisite sensitivity of our GDE-Au substrate for detecting intermediates adsorbed or at least in the close vicinity of the electrode, even for complex mechanisms that display only poorly Raman active intermediates.

Computational Insights: DFT Calculations Including Surface Environment and Electric Potential Dimension. DFT minimum energy calculations at 0 V_{SHE} of the O-dissociated (A) and C-dissociated (B) forms show a competitive stability with an energy difference of about 70 meV in favor of (A) with a pseudo-bridge structure while (B) has a top-one (Figure 4c). The adsorption modes of the two configurations are very different, where the O-dissociated form (B) tends to adopt a pseudo-bridge structure while the C-dissociated one has a top-one. In order to account for more realistic reactive conditions, the surrounding surface environment was described by including an implicit solvent (see SI details) and by the application of a variable electric potential.[46-49] Figure 4d shows the computed free electrochemical energies of (A) and (B) evolving in solvated media[46,48] as function of the applied potential. The results confirm the experiments in neutral pH where α-D-glucose is the most reactive anomer, implying that the enzymatic preference of the β-D anomer[7,9-10] is not always valid. Figure 4d shows that both reactions are slightly exothermic relatively to free solvated glucose and gold surface by about 50 meV. In both systems, the C-O bonds in the hemiacetal moiety remain in the 1.39-1.45 Å range suggesting that the dissociation has no impact on the lactone-like structure. Nevertheless, when including the surface potential dimension, (A) is found to be stable at low potentials and at high potentials for (B) with a stability transition at ca. 0.45 V_{SHE}. This transition is probably the consequence of the large oxygen electronegativity that destabilizes the Au-O bond under

oxidation compared to the slightly more covalent C-Au bond. For $E > 0$ V_{SHE}, the C-dissociated (B) undergoes a bond reorganization with an increase of the Au-C bond length, and at the same time, a reduction of the two O-C bonds attached to this carbon. For $E > 1.1$ V_{SHE}, (B) spontaneously transforms into a carbonyl moiety protonated form ($H\text{-}O^{+}\text{=}C$) of glucono-1,5-lactone (B') that is the cyclic ester form of gluconic acid. The local geometry of C(-C)(-OH)(-O) is found to be planar and the two C-O bonds are decreased to 1.29 Å consistently with the formation of a (cyclic)-ester moiety. Indeed, the C-Au bond reorganization transfers the electron from the Au-C bond to Au surface, thus creating a cationic protonated gluconolactone-like structure. Under the experimental conditions, this cation that is the acidic form of a carbonyl in an ester (p*K*a < -6) should quickly react with a base or water and convert into gluconolactone followed by quick saponification and cycle opening, giving the gluconate anion as experimentally observed by HPLIC and EC-SERS above.

The rationalization of the process can be understood by using the Fukui functions[50] for the two systems that are showing the active redox center, Figures 5a-b. In the configuration A (Figure 5a), mostly all non-bonding oxygen doublets are homogeneously weakly oxidized. In the configuration B (Figure 5b), the C attached to the Au surface and the hemiacetal OH are mostly oxidized; the orbital system that is oxidized correspond to a filled π^* system meaning that the oxidation would lead to the formation a double C=O bond and the formation of the protonated glucosidic ester as computed. The associated classical redox oxidation is then Au-C(OH) → Au-C^{+}(OH) + e^{-} → Au + $C\text{=}O^{+}$-H. Notably, the computed harmonic vibrations of $\upsilon_{C=O}$ band at 1715 cm^{-1} highly concords with the band at 1720 cm^{-1} for gluconolactone intermediate detected by EC-SERS above.

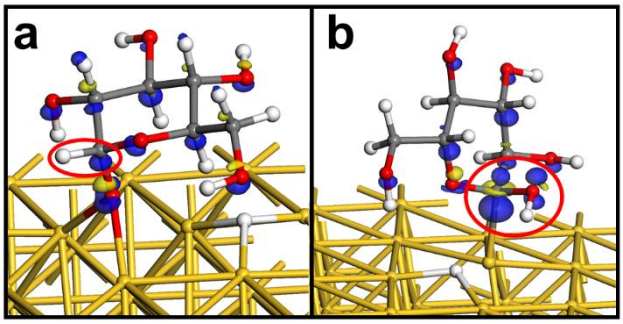

Figure 5. Fukui function for configuration A [O-dissociated form, (a)] and B [C-dissociated form, (b)] showing the active redox center for glucose adsorbed on the Au(111) surface after the first PCET. The blue iso-density gives the localization of the (oxidation) center, while the yellow one is linked with molecular polarization. The iso-densities are the same for the two functions and set to 40 A^{-3}. Color code of atoms: Au in yellow spheres, H in white, O in red, and C in grey.

3. CONCLUSION

In this work, we have developed an accurate methodology to elucidate the electrocatalytic reactivity of glucose anomers at bare Au electrocatalysts. The synthesized bare Au particles directly attached to gas diffusion electrode (GDE) outperformed the existing literature. In-situ electrochemical surface-enhanced Raman spectroscopy has identified gluconolactone as the intermediate during the proton-coupled electron transfer (PCET) process while gluconate is the main product with high selectivity and faradaic efficiency (>80%). α-D-glucose is the most reactive anomer in neutral pH and alkaline pH corresponds to β-D-glucose, which invalidates the traditional thoughts from seminal enzymatic studies that the β-anomer would always be the most reactive. Experimental data were confirmed by potential-dependent energy profiles by density functional theory (DFT) showing that PCET proceeds by the dehydrogenation of the hydrogen of

the OH group bonded to anomeric carbon until 0.45 V_{SHE}. Our findings show that the electrooxidation starts at electrode potentials where the gold surface is not yet nominally oxidized (E_{onset} < 0.3 V_{RHE}), which rules out the hypothesis that glucose first adsorbs on hydroxylated gold surface. The absence of hydroxyl functions on the gold surface promotes an approach by the OH group bonded to the hemiacetal carbon of glucose to produce an intermediate of oxidized-like gold surface after the first PCET. Ongoing studies are focusing on expanding this methodology to extended crystallographic orientations, and re-interrogating the glucose bioelectrocatalysis of model enzymes for electro-energy production. Regarding the electrocatalysts, the striking results obtained with surfactant-free and binder-free gold particles grown on GDE as free-standing electrocatalysts open new avenues to design efficient anodes to drive progress in sustainable electrosynthesis by water-to-hydrogen, CO_2-to-chemicals, and N_2-to-ammonia electrolyzers.

ASSOCIATED CONTENT

Supporting Information.

The Supporting Information is available free of charge at http://pubs.acs.org/. Experimental procedures; computational methods; scenarios for the mechanism of glucose electrooxidation reaction; SEM images; TEM/STEM/EDX images; CVs; EIS data; ICP-OES data; AFM; comparative performance of relevant glucose electrooxidation reaction on metallic catalysts in alkaline media; electrolysis; HPLIC, electrochemical data of redox probe $Fe(CN)_6^{3-}/Fe(CN)_6^{4-}$.

AUTHOR INFORMATION

Corresponding Authors

*Y. H.: E-mail: yaovi.holade@enscm.fr

*H. G.: E-mail: hazar.guesmi@enscm.fr

*T. W. N.: E-mail: teko.napporn@univ-poitiers.fr

*S. D. M.: E-mail: minteer@chem.utah.edu

Notes

The authors declare no competing financial interest.

ACKNOWLEDGMENT

Y. H. acknowledges startup funds support from European Institute of Membranes of Montpellier (COGENFC, PAT-Energy-Axis-2018) and LabEx CheMISyst (ANR-10-LABX-05-01). This work was financially supported by the Army Research Office MURI (W911NF-14-1-0263). This work was also granted access to the HPC resources of [CCRT/CINES/ IDRIS] under the allocation 2020 [x2020087369] made by GENCI (Grand Equipement National de Calcul Intensif). For the materials characterization by Scanning Transmission Electron Microscope (S/TEM: JEOL JEM-2800) and Focused Ion-Beam Dual-Beam Microscopy (dbFIB, FEI Helios NanoLab 650), this work made use of University of Utah USTAR shared facilities support, in part, by the MRSEC Program of NSF under Award No. DMR-1121252. K.S., K.B.K. and T.W.N. thank the "European Union (ERDF)", "Région Nouvelle-Aquitaine" and "Grand Angoulême" for financial supports. We thank Didier Cot, Bertrand Rebiere, and Arie van der Lee of IEM for assistance during SEM, EDX and XRD analysis. We thank Valerie Flaud of ICG Montpellier for XPS characterization. We thank Bastien Michelet of University of Poitiers for help with polarimetry experiments.

REFERENCES

(1) Katz, E.; Willner, I.; Kotlyar, A. B., A non-compartmentalized glucose/O2 biofuel cell by bioengineered electrode surfaces. *J. Electroanal. Chem.* **1999,** *479*, 64-68.

(2) Tsujimura, S.; Murata, K.; Akatsuka, W., Exceptionally High Glucose Current on a Hierarchically Structured Porous Carbon Electrode with "Wired" Flavin Adenine Dinucleotide-Dependent Glucose Dehydrogenase. *J. Am. Chem. Soc.* **2014,** *136*, 14432-14437.

(3) Verma, S.; Lu, S.; Kenis, P. J. A., Co-electrolysis of CO2 and glycerol as a pathway to carbon chemicals with improved technoeconomics due to low electricity consumption. *Nat. Energy* **2019,** *4*, 466-474.

(4) Holade, Y.; Tuleushova, N.; Tingry, S.; Servat, K.; Napporn, T. W.; Guesmi, H.; Cornu, D.; Kokoh, K. B., Recent advances in the electrooxidation of biomass-based organic molecules for energy, chemicals and hydrogen production. *Catal. Sci. Technol.* **2020,** *10*, 3071-3112.

(5) Khan, M. A.; Al-Attas, T. A.; Yasri, N. G.; Zhao, H.; Larter, S.; Hu, J.; Kibria, M. G., Techno-economic analysis of a solar-powered biomass electrolysis pathway for coproduction of hydrogen and value-added chemicals. *Sustainable Energy Fuels* **2020,** *4*, 5568-5577.

(6) Armstrong, R. D.; Hirayama, J.; Knight, D. W.; Hutchings, G. J., Quantitative Determination of Pt- Catalyzed d-Glucose Oxidation Products Using 2D NMR. *ACS Catal.* **2019,** *9*, 325-335.

(7) Oliva, L.; Fernandez-Lopez, J. A.; Remesar, X.; Alemany, M., The anomeric nature of glucose and its implications on its analyses and the influence of diet: are routine glycaemia measurements reliable enough? *J. Endocrinol. Metab.* **2019,** *9*, 63-70.

(8) Okuda, J. U. N.; Taguchi, T.; Tomimura, A., Mutarotation of D-Glucose in Body Fluids and Perfused Rat Liver. *Chem. Pharm. Bull. (Tokyo)* **1987,** *35*, 4332-4337.

(9) Miwa, I.; Maeda, K.; Okuda, J., Anomeric compositions of D-glucose in tissues and blood of rat. *Experientia* **1978,** *34*, 167-169.

(10) Wong, C. M.; Wong, K. H.; Chen, X. D., Glucose oxidase: natural occurrence, function, properties and industrial applications. *Appl. Microbiol. Biotechnol.* **2008,** *78*, 927-938.

(11) Hickey, D. P.; Milton, R. D.; Rasmussen, M.; Abdellaoui, S.; Nguyen, K.; Minteer, S. D. In *Electrochemistry: Volume 13*, The Royal Society of Chemistry: 2016; Vol. 13, pp 97-132.

(12) Largeaud, F.; Kokoh, K. B.; Beden, B.; Lamy, C., On the electrochemical reactivity of anomers: electrocatalytic oxidation of α- and β-d-glucose on platinum electrodes in acid and basic media. *J. Electroanal. Chem.* **1995,** *397*, 261-269.

(13) Hsiao, M. W.; Adžić, R. R.; Yeager, E. B., Electrochemical Oxidation of Glucose on Single Crystal and Polycrystalline Gold Surfaces in Phosphate Buffer. *J. Electrochem. Soc.* **1996,** *143*, 759-767.

(14) Holade, Y.; Servat, K.; Napporn, T. W.; Morais, C.; Berjeaud, J.-M.; Kokoh, K. B., Highly Selective Oxidation of Carbohydrates in an Efficient Electrochemical Energy Converter: Cogenerating Organic Electrosynthesis. *ChemSusChem* **2016,** *9*, 252-263.

(15) Caglar, A.; Düzenli, D.; Onal, I.; Tezsevin, I.; Sahin, O.; Kivrak, H., A comparative experimental and density functional study of glucose adsorption and electrooxidation on the Au-graphene and Pt-graphene electrodes. *Int. J. Hydrogen Energy* **2020,** *45*, 490-500.

(16) Ishimoto, T.; Kazuno, H.; Kishida, T.; Koyama, M., Theoretical study on oxidation reaction mechanism on Au catalyst in direct alkaline fuel cell. *Solid State Ionics* **2014,** *262*, 328-331.

(17) Hebié, S.; Holade, Y.; Maximova, K.; Sentis, M.; Delaporte, P.; Kokoh, K. B.; Napporn, T. W.; Kabashin, A. V., Advanced Electrocatalysts on the Basis of Bare Au Nanomaterials for Biofuel Cell Applications. *ACS Catal.* **2015,** *5*, 6489-6496.

(18) Xu, M.; Sui, Y.; Xiao, G.; Yang, X.; Wei, Y.; Zou, B., Kinetically controlled synthesis of nanoporous Au and its enhanced electrocatalytic activity for glucose-based biofuel cells. *Nanoscale* **2017,** *9*, 2514-2520.

(19) Wang, J.; Gong, J.; Xiong, Y.; Yang, J.; Gao, Y.; Liu, Y.; Lu, X.; Tang, Z., Shape-dependent electrocatalytic activity of monodispersed gold nanocrystals toward glucose oxidation. *Chem. Commun.* **2011,** *47*, 6894-6896.

(20) Wang, Z.; Liu, P.; Han, J.; Cheng, C.; Ning, S.; Hirata, A.; Fujita, T.; Chen, M., Engineering the internal surfaces of three-dimensional nanoporous catalysts by surfactant-modified dealloying. *Nat. Commun.* **2017,** *8*, 1066.

(21) Wei, L.; Sheng, T.; Ye, J.-Y.; Lu, B.-A.; Tian, N.; Zhou, Z.-Y.; Zhao, X.-S.; Sun, S.-G., Seeds and Potentials Mediated Synthesis of High-Index Faceted Gold Nanocrystals with Enhanced Electrocatalytic Activities. *Langmuir* **2017,** *33*, 6991-6998.

(22) Liu, B.; Greeley, J., Decomposition Pathways of Glycerol via C–H, O–H, and C–C Bond Scission on Pt(111): A Density Functional Theory Study. *J. Phys. Chem. C* **2011,** *115*, 19702-19709.

(23) Garcia, A. C.; Kolb, M. J.; van Nierop y Sanchez, C.; Vos, J.; Birdja, Y. Y.; Kwon, Y.; Tremiliosi-Filho, G.; Koper, M. T. M., Strong Impact of Platinum Surface Structure on Primary and Secondary Alcohol Oxidation during Electro-Oxidation of Glycerol. *ACS Catal.* **2016,** *6*, 4491-4500.

(24) Rizo, R.; Roldan Cuenya, B., Shape-Controlled Nanoparticles as Anodic Catalysts in Low-Temperature Fuel Cells. *ACS Energy Lett.* **2019,** *4*, 1484-1495.

(25) Higgins, D.; Hahn, C.; Xiang, C.; Jaramillo, T. F.; Weber, A. Z., Gas-Diffusion Electrodes for Carbon Dioxide Reduction: A New Paradigm. *ACS Energy Lett.* **2018,** *4*, 317-324.

(26) Rafaïdeen, T.; Baranton, S.; Coutanceau, C., Highly efficient and selective electrooxidation of glucose and xylose in alkaline medium at carbon supported alloyed PdAu nanocatalysts. *Appl. Catal. B: Env.* **2019,** *243*, 641-656.

(27) Lepage, T.; Kammoun, M.; Schmetz, Q.; Richel, A., Biomass-to-hydrogen: A review of main routes production, processes evaluation and techno-economical assessment. *Biomass Bioenergy* **2021,** *144*, 105920.

(28) Morandi, P.; Tuleushova, N.; Tingry, S.; Cambedouzou, J.; Minteer, S. D.; Cornu, D.; Holade, Y., Bromide-Regulated Anisotropic Growth of Desert-Rose-Like Nanostructured Gold onto Carbon Fiber Electrodes as Freestanding Electrocatalysts. *ACS Appl. Energy Mater.* **2020,** *3*, 7560-7571.

(29) Holade, Y.; Hickey, D. P.; Minteer, S. D., Halide-regulated growth of electrocatalytic metal nanoparticles directly onto a carbon paper electrode. *J. Mater. Chem. A* **2016,** *4*, 17154-17162.

(30) Xin, W.; Severino, J.; De Rosa, I. M.; Yu, D.; McKay, J.; Ye, P.; Yin, X.; Yang, J.-M.; Carlson, L.; Kodambaka, S., One-Step Synthesis of Tunable-Size Gold Nanoplates on Graphene Multilayers. *Nano Lett.* **2018,** *18*, 1875-1881.

(31) Siegmund, D.; Metz, S.; Peinecke, V.; Warner, T. E.; Cremers, C.; Grevé, A.; Smolinka, T.; Segets, D.; Apfel, U.-P., Crossing the Valley of Death: From Fundamental to Applied Research in Electrolysis. *JACS Au* **2021,** *1*, 527-535.

(32) Xu, D.; Stevens, M. B.; Cosby, M. R.; Oener, S. Z.; Smith, A. M.; Enman, L. J.; Ayers, K. E.; Capuano, C. B.; Renner, J. N.; Danilovic, N.; Li, Y.; Wang, H.; Zhang, Q.; Boettcher, S. W., Earth-Abundant Oxygen Electrocatalysts for Alkaline Anion-Exchange-Membrane Water

Electrolysis: Effects of Catalyst Conductivity and Comparison with Performance in Three-Electrode Cells. *ACS Catal.* **2019,** *9*, 7-15.

(33) Weber, M.; Tuleushova, N.; Zgheib, J.; Lamboux, C.; Iatsunskyi, I.; Coy, E.; Flaud, V.; Tingry, S.; Cornu, D.; Miele, P.; Bechelany, M.; Holade, Y., Enhanced electrocatalytic performance triggered by atomically bridged boron nitride between palladium nanoparticles and carbon fibers in gas-diffusion electrodes. *Appl. Catal. B: Env.* **2019,** *257*, 117917.

(34) Wang, X.; Li, Y.; Jin, T.; Meng, J.; Jiao, L.; Zhu, M.; Chen, J., Electrospun Thin-Walled CuCo2O4@C Nanotubes as Bifunctional Oxygen Electrocatalysts for Rechargeable Zn–Air Batteries. *Nano Lett.* **2017,** *17*, 7989-7994.

(35) Ayers, K. E.; Renner, J. N.; Danilovic, N.; Wang, J. X.; Zhang, Y.; Maric, R.; Yu, H., Pathways to ultra-low platinum group metal catalyst loading in proton exchange membrane electrolyzers. *Catal. Today* **2016,** *262*, 121-132.

(36) Zhao, Z.; Qin, F.; Kasiraju, S.; Xie, L.; Alam, M. K.; Chen, S.; Wang, D.; Ren, Z.; Wang, Z.; Grabow, L. C.; Bao, J., Vertically Aligned MoS2/Mo2C hybrid Nanosheets Grown on Carbon Paper for Efficient Electrocatalytic Hydrogen Evolution. *ACS Catal.* **2017,** *7*, 7312-7318.

(37) Negro, E.; Latsuzbaia, R.; Dieci, M.; Boshuizen, I.; Koper, G. J. M., Pt electrodeposited over carbon nano-networks grown on carbon paper as durable catalyst for PEM fuel cells. *Appl. Catal. B: Env.* **2015,** *166–167*, 155-165.

(38) Ehelebe, K.; Schmitt, N.; Sievers, G.; Jensen, A. W.; Hrnjić, A.; Collantes Jiménez, P.; Kaiser, P.; Geuß, M.; Ku, Y.-P.; Jovanovič, P.; Mayrhofer, K. J. J.; Etzold, B.; Hodnik, N.; Escudero-Escribano, M.; Arenz, M.; Cherevko, S., Benchmarking Fuel Cell Electrocatalysts Using Gas Diffusion Electrodes: Inter-lab Comparison and Best Practices. *ACS Energy Lett.* **2022,** *7*, 816-826.

(39) Bard, A. J.; Faulkner, L. R., *Electrochemical Methods: Fundamentals and Applications*. 2nd ed.; John Wiley & Sons, Inc.: USA, 2001; p 850.

(40) Wang, J.; Chen, F.; Jin, Y.; Lei, Y., Dilute Au-Containing Ag Nanosponges as a Highly Active and Durable Electrocatalyst for Oxygen Reduction and Alcohol Oxidation Reactions. *ACS Appl. Mater. Interfaces.* **2018,** *10*, 6276-6287.

(41) Mathlouthi, M.; Vinh Luu, D., Laser-raman spectra of d-glucose and sucrose in aqueous solution. *Carbohydr. Res.* **1980,** *81*, 203-212.

(42) Söderholm, S.; Roos, Y. H.; Meinander, N.; Hotokka, M., Raman spectra of fructose and glucose in the amorphous and crystalline states. *J. Raman Spectrosc.* **1999,** *30*, 1009-1018.

(43) Holade, Y.; Engel, A. B.; Servat, K.; Napporn, T. W.; Morais, C.; Tingry, S.; Cornu, D.; Kokoh, K. B., Electrocatalytic and Electroanalytic Investigation of Carbohydrates Oxidation on Gold-Based Nanocatalysts in Alkaline and Neutral pHs. *J. Electrochem. Soc.* **2018,** *165*, H425-H436.

(44) Sung, C.-J.; Chao, S.-H.; Hsu, S.-C., Rapid Detection of Glucose on Nanostructured Gold Film Biosensor by Surface-Enhanced Raman Spectroscopy. *Biosensors* **2021,** *11*, 54.

(45) Smith, S. R.; Seenath, R.; Kulak, M. R.; Lipkowski, J., Characterization of a Self-Assembled Monolayer of 1-Thio-β-d-Glucose with Electrochemical Surface Enhanced Raman Spectroscopy Using a Nanoparticle Modified Gold Electrode. *Langmuir* **2015,** *31*, 10076-10086.

(46) Kopač Lautar, A.; Hagopian, A.; Filhol, J.-S., Modeling interfacial electrochemistry: concepts and tools. *Phys. Chem. Chem. Phys.* **2020,** *22*, 10569-10580.

(47) Filhol, J.-S.; Neurock, M., Elucidation of the Electrochemical Activation of Water over Pd by First Principles. *Angew. Chem. Int. Ed.* **2006,** *45*, 402-406.

(48) Mamatkulov, M.; Filhol, J. S., An abinitio study of electrochemical vs. electromechanical properties: the case of CO adsorbed on a Pt(111) surface. *Phys. Chem. Chem. Phys.* **2011,** *13*, 7675-7684.

(49) Lespes, N.; Filhol, J.-S., Using Implicit Solvent in Ab Initio Electrochemical Modeling: Investigating Li+/Li Electrochemistry at a Li/Solvent Interface. *J. Chem. Theory Comput.* **2015,** *11*, 3375-3382.

(50) Lautar, A. K.; Hagopian, A.; Filhol, J.-S., Modeling interfacial electrochemistry: concepts and tools. *Phys. Chem. Chem. Phys.* **2020,** *22*, 10569-10580.